Characterization of phase structures in semiconducting $SnWO_4$ powders by Mössbauer and Raman spectroscopies

J. L. Solis,* J. Frantti, and V. Lantto
Microelectronics Laboratory, University of Oulu, Linnanmaa, FIN-90571 Oulu, Finland

L. Häggström and M. Wikner
Department of Physics, Uppsala University, P.O. Box 530, 751 21 Uppsala, Sweden

(Received 20 January 1998)

Stannous tungstate, $SnWO_4$, crystallizes in the low-temperature α and high-temperature β phases. α-$SnWO_4$ powders were prepared by heating an equimolar mixture of SnO and WO_3 either in vacuum or in argon atmosphere at 600 °C for 15 h. The high-temperature β phase was obtained as metastable at room temperature after heating the mixture at 800 °C and rapid quenching. In addition to x-ray-diffraction studies, ^{119}Sn Mössbauer and Raman spectroscopies were used as ''local'' probes for the characterization of the phase structures in the semiconducting and gas-sensitive powders. The composition of the powders was measured by the energy-dispersive spectroscopy of x rays. Mössbauer spectroscopy, especially, as a very local probe for tin atoms gave valuable information of small extra phase(s) in the α- and β-$SnWO_4$ powders originating in the oxidation of Sn^{2+} ions in the $SnWO_4$ structures into the Sn^{4+} form. The Sn^{2+} Mössbauer doublet from both α and β phases showed some asymmetry not published before. The asymmetry was possible to relate to the Goldanskii-Karyagin effect with calculations based on published results for the atomic positions and thermal displacement parameters in the x-ray temperature factor of the α- and β-$SnWO_4$ structures. Raman spectra are given together with peak frequencies from a curve fit for both α- and β-phase powders. The symmetries and selection rules of the normal modes at the center of the Brillouin zone are also given for both α and β phases. [S0163-1829(98)00721-8]

I. INTRODUCTION

Jeitschko and Sleight[1] reported the fabrication of $SnWO_4$ from SnO and WO_3 powders as two varieties, the low-temperature α phase and high-temperature β phase, which transform into each other by a fast, but diffusion-controlled phase-transition mechanism at 670 °C. The decomposition of the α-$SnWO_4$ phase during heating in air starts at temperatures above about 550 °C,[2] while the metastable β-$SnWO_4$, after a rapid quenching from above 670 °C, decomposes in air at temperatures above about 450 °C.[3] The fabrication of the α phase is possible also in the form of thin films by sputtering.[4] In the orthorhombic crystal structure of α-$SnWO_4$ both metal atoms have distorted octahedral oxygen coordinations as in SnO_2 and WO_3, whereas in the cubic structure of the β phase tungsten atoms sit inside oxygen tetrahedra which are not linked.[1,5] However, in contrast to SnO_2, tin appears in the divalent form Sn^{2+} in both α and β structures. There are only a few reports of stannous tungstate in the literature.

Both SnO_2 and WO_3 are well-known materials in the field of gas-sensing[6] and electrochromic[7] applications. They are extrinsic n-type semiconductors similarly with the α and β phases of $SnWO_4$ which are also gas-sensitive oxides. The electrical conductivity of these oxides changes with concentrations of some gas components in the ambient atmosphere which is the basis for gas sensing with semiconductor gas sensors. However, electrical and gas-response properties of $SnWO_4$ powders are very sensitive to the process and conditions which are used for the fabrication of the material. The easy oxidation of Sn^{2+} into the Sn^{4+} form may generate some extra phase(s), especially, at the grain surfaces which may have a strong influence on the gas-sensing properties of the material.

Here we use ^{119}Sn Mössbauer and Raman spectroscopies together with x-ray diffraction (XRD) measurements and energy-dispersive spectroscopy (EDS) analyses for the structure characterization of α- and β-$SnWO_4$ powders fused from SnO and WO_3 powders both in vacuum and in argon atmospheres. In the case of very small crystals, e.g., from an extra phase at the grain surfaces, structural information from XRD and Raman results may seem confusing, since x-ray-diffraction probes long-range order whereas Raman is, in principle, a ''local'' probe.[8] Mössbauer spectroscopy, on the other hand, is a very useful local probe, based on hyperfine interactions, for the study of possible small extra phase(s) originating in the oxidation of Sn^{2+} ions in the $SnWO_4$ structures into the Sn^{4+} form.

II. CRYSTAL STRUCTURES AND ATOMIC DISPLACEMENTS

Crystal structure is the basis for the interpretation of Raman results (phonon symmetries) and XRD patterns. In addition, a knowledge of the lattice vibrations (atomic displacements) is very important for the interpretation of Mössbauer spectra. Here we use the results of Jeitschko and Sleight[1,5] for the crystal structure and thermal displacement parameters of α- and β-$SnWO_4$ at room temperature. α-$SnWO_4$ has an orthorhombic crystal structure with the space group

 © 1998 The American Physical Society

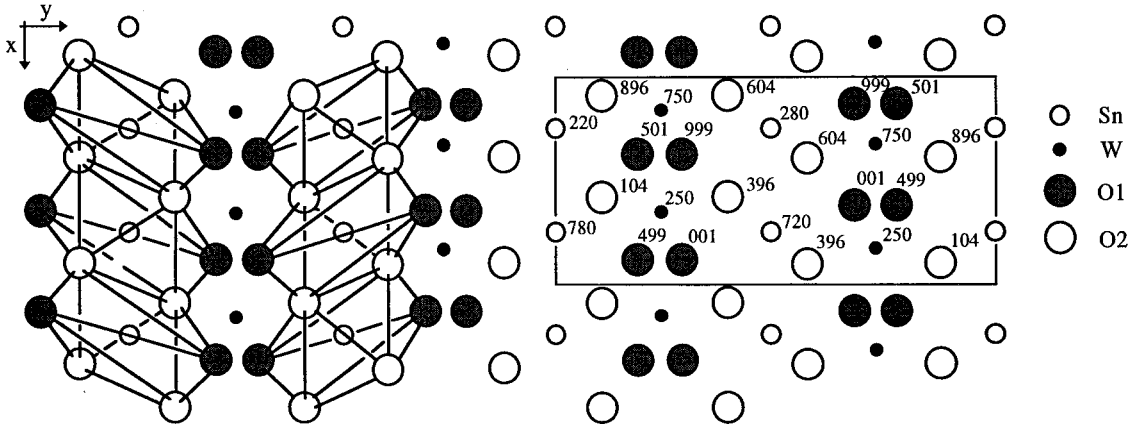

FIG. 1. Projection of the α-$SnWO_4$ structure. The distorted SnO_6 octahedra are shown on the left and the unit cell on the right. The atomic positions together with the z coordinates ($\times 10^3$) in the unit cell are from Ref. 5.

$D_{2h}^6(P_{nna})$ and lattice constants $a=5.6270(3)$ Å, $b=11.6486(7)$ Å, and $c=4.9973(3)$ Å. The unit cell contains four formula units. Figure 1 shows a projection of the structure in the z direction. The positions of the atoms are from Jeitschko and Sleight.[5] The distorted SnO_6 octahedra are also shown in Fig. 1, and the distorted WO_6 octahedra (not shown in Fig. 1) are linked at the four corners. In this manner, they form sheets of $[WO_4]^{2-}$ polyanions which are held together by Sn atoms with the formal valency of $+2$. The dark-red color of α-$SnWO_4$ could be due to the charge transfer involving an electron transfer from Sn^{2+} to W^{6+} (Ref. 5). A value of 3.05 eV was obtained for the band gap E_g corresponding to direct allowed transitions from spectral optical constants n and k computed for an α-$SnWO_4$ thin film in the visible range from measured spectral transmittance and reflectance data.[9] No results were found in the literature for the electronic structure of α-$SnWO_4$ from band-structure calculations.

The temperature factor $T_l(\mathbf{H})$ of the lth atom in the unit cell at the x-ray reflection $\mathbf{H}$, in the expression for the structure factor $F(\mathbf{H})$, has the general expression for a harmonic crystal[10]

$$T_l(\mathbf{H})=\exp(-2\pi^2\mathbf{H}^T B(l)\mathbf{H}), \tag{1}$$

where $B(l)=\langle \mathbf{u}(l)\cdot(\mathbf{u}(l))^T\rangle$ is the mean-square displacement matrix of the lth atom. The element $\langle u_i u_j\rangle$ represents the average value of the atomic displacements along the Cartesian i axis multiplied by the displacements along the j axis. Usually, least-squares refinement programs yield a list of the anisotropic temperature-factor coefficients β_{ij} for the atoms in the unit cell because the mean position of the atom l in the unit cell is not usually introduced in terms of its Cartesian components, but rather as fractional coordinates of the unit-cell axes **a**, **b**, and **c**. The temperature factor now takes the form

$$T_l(\mathbf{H})=\exp\left(-\sum_i \sum_j h_i h_j \beta_{ij_l}\right), \tag{2}$$

where h_i and h_j refer to the reciprocal-lattice vector $\mathbf{H}$. β is a symmetric matrix whose dimensionless elements are defined with respect to the unit-cell axes. The relationship between B and β is[10] $B=(1/2\pi^2)F^T\beta F$, where the upper-triangular matrix F has the lengths of the unit-cell axes as elements on the main diagonal and all off-diagonal elements are zero in the case of orthorhombic (and cubic) lattice. The anisotropic temperature-factor coefficients β_{ij} are given for Sn, W, O(1), and O(2) atoms (Fig. 1) of the α-$SnWO_4$ structure at room temperature in Ref. 5 [β_{ij}'s are isotropic for O(1) and O(2) atoms].

β-$SnWO_4$ has a cubic crystal structure with the space group T^4 ($P2_13$) and a lattice constant $a=7.2989(3)$ Å.[1] The unit cell contains four formula units. Figure 2 shows a projection of the structure in the z direction. The positions of the atoms are from Jeitschko and Sleight.[1] The distorted SnO_6 octahedra around the Sn atoms are also shown in Fig. 2. The structure can be described as an arrangement of $[WO_4]^{2-}$ tetrahedra interspersed with Sn^{2+} ions. The $[WO_4]^{2-}$ tetrahedra are not connected, i.e., they do not share oxygen atoms. The W, Sn, and O(1) atoms in Fig. 2 are situated on the threefold axes (main diagonals) of the unit cell, while the O(2) atoms in the general positions fill the remaining places. The anisotropic temperature-factor coefficients β_{ij} are given for Sn, W, O(1), and O(2) atoms (Fig. 2) at room temperature in Ref. 1 [β_{ij}'s are isotropic for O(1) and O(2) atoms].

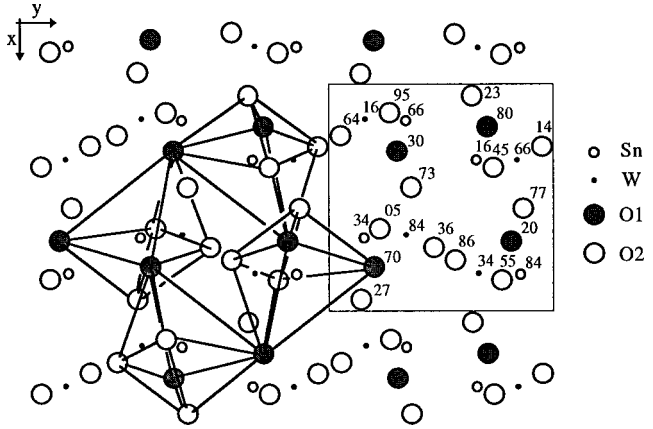

FIG. 2. Projection of the β-$SnWO_4$ structure. The distorted SnO_6 octahedra are shown on the left and the unit cell on the right. The atomic positions together with the z coordinates ($\times 10^2$) in the unit cell are from Ref. 1.

III. EXPERIMENT

The fabrication of stannous tungstate powder began by mixing equimolar quantities of SnO and WO_3 powders and by ball milling in acetone for 1 h. For the synthesis of α-$SnWO_4$ powder the mixture was sealed in a silica tube in vacuum and heated at 600 °C for 15 h. Another method to obtain fusion was to heat the mixture in an argon atmosphere at 600 °C for 15 h. The high-temperature β phase was obtained as metastable at room temperature by a rapid quenching of the mixture sealed in an evacuated silica tube after heating at 800 °C for 15 h and slow cooling to 700 °C. ^{119}Sn Mössbauer spectroscopy studies were carried out at room temperature with a Mössbauer spectrometer working in the acceleration mode with sources on each side of the vibrator. The velocity calibration spectrum was measured with a ^{57}CoRh source and an α-Fe absorber at room temperature. The source used for the ^{119}Sn spectrum was $Ca^{119}SnO_3$ (2 mCi).

Mössbauer spectra in the transmission geometry were measured from samples with the amount of Sn of around 30 mg cm^{-2} in the radiation direction. To spread out the stannous tungstate powder over the whole measuring area the sample was mixed with BN to form a homogeneous mass. This was, in turn, pressed into a 2-mm-thick plate kept in the holder by a thin aluminium layer on each side of the plate. To avoid texture effects the measurement was conducted at the ''magic angle'' (54.7°).[11]

To obtain more information about the α-$SnWO_4$ structure two further experiments were conducted. The samples used contained the α-$SnWO_4$ powder fused in vacuum, since this powder had narrower line width [full width at half maximum (FWHM)] than the one fused in the argon atmosphere. An experiment was carried out on a cube (1 cm^3) which was gently filled with BN and 13 mg Sn per cm^3. Measurements were made in the x, y, and z directions in order to check possible texture effects. The second experiment was conducted on a plate with only 3 mg Sn per cm^2 to minimize saturation effects.

Raman-scattering measurements were performed at room temperature using the Jobin Yvon T-6400 triple Raman spectrometer equipped with a CCD detector. An Ar-ion laser with a wavelength of 514.532 nm was employed and the measurements were carried out with the backscattering configuration. The micro-Raman utility was used to measure the spectra under a microscope. The Raman spectra were measured from discs of pressed powders with a diameter of 1 cm.

X-ray diffraction (XRD) and EDS were used for the characterization of the crystal structure and composition of the stannous tungstate powders, respectively. EDS measurements were performed using the JEOL JSM-6400/LINK AN 10-85 spectrometer and the Philips PW 1353/00 diffractometer with Cu $K\alpha$ radiation was used for the recording of XRD patterns.

For electrical and gas-response measurements some thick-film samples were made from various $SnWO_4$ powders by screen printing on alumina substrates having preprinted gold electrodes and a Pt-heating resistor on the reverse side of the substrate.

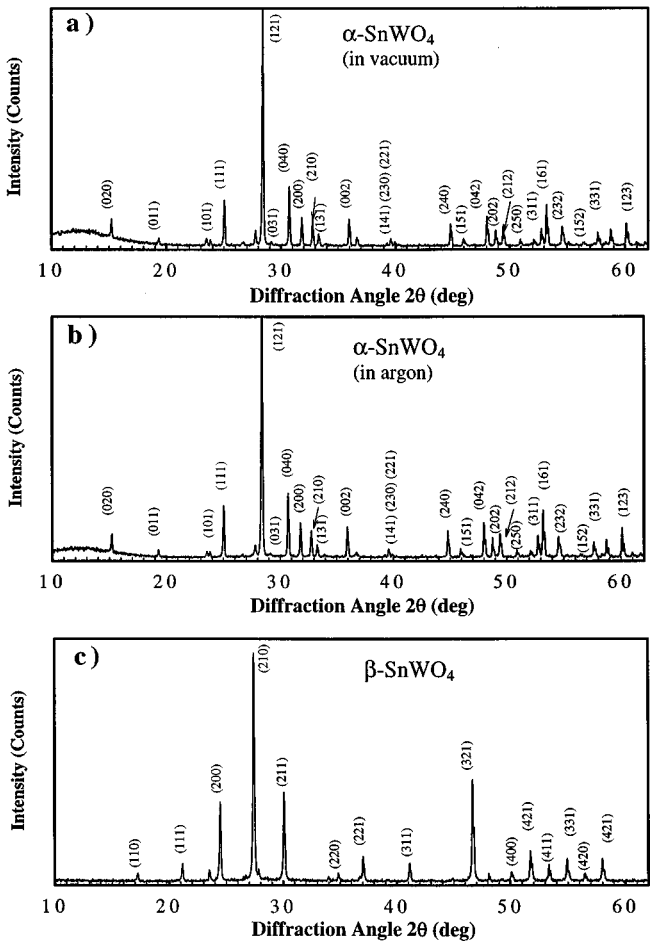

FIG. 3. XRD patterns from α-$SnWO_4$ powders fused (a) in vacuum and (b) in argon, and (c) from metastable β-$SnWO_4$ powder fused in vacuum.

IV. RESULTS AND DISCUSSION

A. XRD and EDS experiments

X-ray-diffraction patterns measured from α- and β-$SnWO_4$ powders are shown in Fig. 3. Figures 3(a) and 3(b) show the patterns from the α-$SnWO_4$ powders fused in vacuum and in argon atmosphere, respectively. The identification of the α-$SnWO_4$ phase is not ambiguous since practically all reflections in both patterns belong to this phase. In addition, the patterns are very identical to each other and it is impossible to see any differences in the structure of the two powders. An estimate for the average grain size of the powders is possible to obtain from the patterns by the Scherrer's formula. It gave the same value of about 40 nm for the average grain size in both α-$SnWO_4$ powders in Fig. 3. However, there were considerable differences in the electrical and gas-response properties between the two powders.[2]

The XRD pattern from the metastable β-$SnWO_4$ powder fused in vacuum is shown in Fig. 3(c). The identification of the high-temperature β phase is also not ambiguous. Some very small reflections, e.g., from the rutile structure of SnO_2 at the 2θ angles of 26.6°, 33.9°, and 51.8°, are seen in the pattern in Fig. 3(c). The average grain size of the β-$SnWO_4$ powder was also about 40 nm. The EDS results for the composition of both α- and β-phase powders and screen-printed thick films agreed with the chemical formula unit $SnWO_4$.

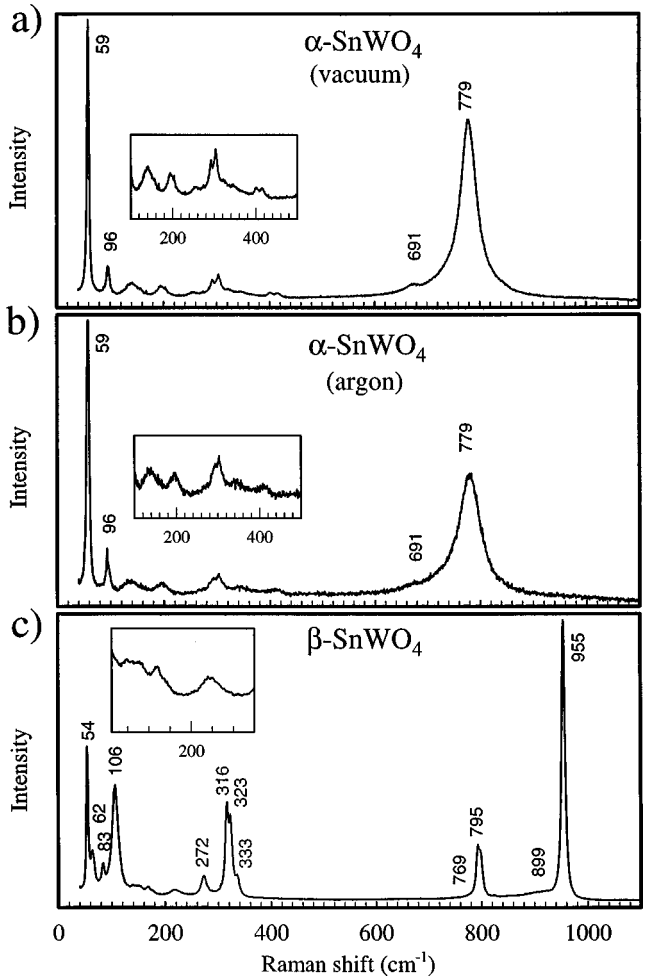

FIG. 4. Raman spectra from α-$SnWO_4$ powders fused (a) in vacuum and (b) in argon, and (c) from metastable β powder fused in vacuum.

B. Raman experiments

The characteristic Raman spectra of the α-$SnWO_4$ powders fused in vacuum and in argon atmosphere, respectively, in Figs. 4(a) and 4(b) are very similar, except for the intensities. In the case of the vacuum-fused powder, the intensity of the Raman peaks is higher and the spectrum is more detailed with narrower peak widths. The spectra were fitted with a curve fit program in order to determine the frequencies of the peaks. The results from the peak fit are seen in Fig. 4 for the main peaks. The α-$SnWO_4$ structure has a strong Raman mode at $779\ cm^{-1}$ and a narrow one at $59\ cm^{-1}$. Sixteen peaks were obtained from the fit of the spectra for the α phase.

The Raman spectrum from the β-$SnWO_4$ powder fused in vacuum is shown in Fig. 4(c) together with peak frequencies from the curve fit. The β-$SnWO_4$ structure shows more resolved peaks than the α phase. It shows two characteristic narrow peaks, one at a high frequency of $955\ cm^{-1}$ and another at a low frequency of $54\ cm^{-1}$. There were 16 peaks that were obtained from the fit of the spectrum. Raman spectra from the initial SnO and WO_3 powders together with a spectrum from the SnO_2 cassiterite structure (rutile-type) are shown in Fig. 5, for comparison. The Raman peaks in the spectra from the tin oxides in Fig. 5 are very weak as compared with the peaks in the spectrum of the WO_3 powder. Therefore, the main peaks in the Raman spectra of α- and β-$SnWO_4$ may originate in the phonons which are closely related to the vibrations of tungsten atoms.

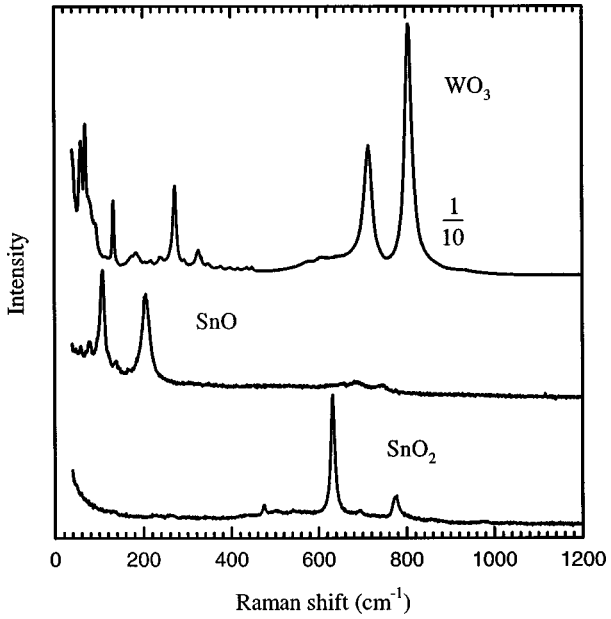

FIG. 5. Raman spectra from WO_3, SnO, and SnO_2 powders. The intensity values of the WO_3 spectrum are multiplied by a factor of 1/10.

No data was found in the literature for the Raman spectra and phonon symmetries in the $SnWO_4$ phases. Therefore, we determined the symmetries for the normal modes at the center Γ of the Brillouin zone in α- and β-$SnWO_4$. Now, the group theory considerations are restricted to those normal modes transforming as the irreducible representations of the point group of the space group, which is isomorphic to the little group at $\mathbf{k}=\mathbf{0}$. For the determination of the phonon symmetries at Γ it is possible to use the mechanical or Δ representation at $\mathbf{k}=\mathbf{0}$. It is a $3r\times 3r$ matrix representation $\Delta^{(\Gamma)}$, where r is the number of atoms in the crystal basis ($r=4\times 6=24$ in both α- and β-$SnWO_4$).

The reduction of the representation $\Delta^{(\Gamma)}$ into a direct sum of allowable irreducible representations of the point group of the space group determines the specific representations related to the symmetry of all normal modes which occur at the zone center Γ, where the little group is the factor group of the space group with respect to the crystal translation group. The number of times a_j, the jth irreducible representation, appears in the direct-sum reduction of $\Delta^{(\Gamma)}$ is given by the equation

$$a_j = h^{-1}\sum_{\kappa=1}^{m} N_\kappa[\chi^{(j)}(C_\kappa)]^{*}\chi^{(\Delta)^{(\Gamma)}}(C_\kappa), \qquad (3)$$

where h is the order of the point group, m is the number of classes in the point group, N_κ is the number of elements in the class C_κ, and $\chi^{(j)}(C_\kappa)$, and $\chi^{(\Delta)^{(\Gamma)}}(C_\kappa)$ are the characters of the elements in the class C_κ in the jth irreducible representation of the point group and mechanical representation $\Delta^{(\Gamma)}$, respectively. Values of $\chi^{(j)}(C_\kappa)$ for different j

TABLE I. Character table together with normal modes at $\mathbf{k}=\mathbf{0}$ and selection rules for α-$SnWO_4$. Bases of the irreducible representations of the point group D_{2h} are also given. R and IR indicate Raman-active and IR-active modes, respectively. $t_0=(000)$; $t_1=(a/2\ 00)$; $t_2=(0\ b/2\ 0)$; $t_3=(a/2\ 0\ c/2)$; $t_4=(0\ b/2\ c/2)$.

Space group D_{2h}^6 Irreps (and $\Delta^{(\Gamma)}$)	Basis	Group operations								Modes at $\mathbf{k}=\mathbf{0}$		
		$\{E\|t_0\}$	$\{C_{2z}\|t_0\}$	$\{C_{2y}\|t_2\}$	$\{C_{2x}\|t_0\}$	$\{I\|t_0\}$	$\{\sigma_z\|t_1\}$	$\{\sigma_y\|t_3\}$	$\{\sigma_x\|t_4\}$	Acoustic	Optic	R/IR
A_g	x^2,y^2,z^2	1	1	1	1	1	1	1	1		8	R
B_{1g}	xy	1	1	−1	−1	1	1	−1	−1		9	R
B_{2g}	xz	1	−1	1	−1	1	−1	1	−1		10	R
B_{3g}	yz	1	−1	−1	1	1	−1	−1	1		9	R
A_u	xyz	1	1	1	1	−1	−1	−1	−1		8	
B_{1u}	z	1	1	−1	−1	−1	−1	1	1	1	8	IR
B_{2u}	y	1	−1	1	−1	−1	1	−1	1	1	9	IR
B_{3u}	x	1	−1	−1	1	−1	1	1	−1	1	8	IR
$\Delta^{(\Gamma)}$		72	−4	0	−4	0	0	0	0			

and κ are given in standard character tables. The character (trace) of the representation $\Delta^{(\Gamma)}$ for the operation $\{\varphi|t\}$ is given by the equation[12]

$$\chi^{(\Delta)^{(\Gamma)}}(C_\kappa)(\{\varphi|t\})=\pm(1+2\cos\varphi)\sum_{\kappa=1}^{r}\delta_{\kappa,\kappa_{\bar{\varphi}}}, \qquad (4)$$

where each of the basis indices κ and $\kappa_{\bar{\varphi}}$ refer to one of the r basis atoms and

$$\delta_{\kappa,\kappa_{\bar{\varphi}}}=\begin{cases}1, & \text{if } \kappa \text{ and } \kappa_{\bar{\varphi}} \text{ are identical basis nuclei}\\ & \text{belonging to the same Bravais sublattice.}\\ 0 & \text{otherwise,}\end{cases}$$

The sum gives the number of basis particles left unchanged, or sent into equivalent particles in the same Bravais sublattice. The other factor in Eq. (4) arises from the trace of the rotation matrix where φ is the angle of rotation of the operation $\{\varphi|0\}$. The $\pm$ is for the proper/improper element, respectively. In the case of symmorphic structure of the space group, it is possible to write Eq. (4) at $\mathbf{k}=\mathbf{0}$ in the simple form

$$\chi^{(\Delta)^{(\Gamma)}}(\{\varphi|0\})=\pm n(\varphi)(1+2\cos\varphi), \qquad (5)$$

where $n(\varphi)$ is the number of basis atoms left unchanged by the element $\{\varphi|0\}$. The use of character tables[13,14] together with Eq. (3) and characters of $\Delta^{(\Gamma)}$, calculated either with Eqs. (4) or (5), makes it possible to reduce the mechanical representation into a direct sum of the irreducible representations of the point group of the space group.

The space group of the orthorhombic α phase of $SnWO_4$ is the nonsymmorphic D_{2h}^6 with the point group D_{2h}. The character table of the point group D_{2h} together with the characters of the mechanical representation $\Delta^{(\Gamma)}$, calculated by Eq. (4), are shown in Table I. The direct-sum reduction of the mechanical representation $\Delta^{(\Gamma)}$ is $8A_g\oplus 9B_{1g}\oplus 10B_{2g}\oplus 9B_{3g}\oplus 8A_u\oplus 9B_{1u}\oplus 10B_{2u}\oplus 9B_{3u}$, as calculated from the characters in Table I with Eq. (3). The group operations given in Table I are performed with respect to different origins which are given in the International Tables for x-ray crystallography. Even (gerade) representations only are Raman active, and three acoustic modes correspond to a representation $B_{1u}\oplus B_{2u}\oplus B_{3u}$. Optical modes B_{1u}, B_{2u}, and B_{3u} are IR active and eight optical A_u modes are silent. In all, we have the direct sum reduction $8A_g\oplus 9B_{1g}\oplus 10B_{2g}\oplus 9B_{3g}\oplus 8A_u\oplus 8B_{1u}\oplus 9B_{2u}\oplus 8B_{3u}$ for the 69 optical normal modes, of which 36 are Raman active.

The space group of the cubic β phase of $SnWO_4$ is the nonsymmorphic T^4 with the point group T. The character table of the point group T together with the characters of the mechanical representation $\Delta^{(\Gamma)}$, calculated from Eq. (4), are shown in Table II. The direct-sum reduction of the mechanical representation is $6\Gamma_1\oplus 6\Gamma_2\oplus 6\Gamma_3\oplus 18\Gamma_4$, as calculated from the characters in Table II with Eq. (3). The group operations given in Table II are all performed with respect to the same origin (Fig. 2). Optical modes Γ_1 (or A in Mulliken notation), Γ_2 and Γ_3 are Raman active and the modes Γ_4 are only IR active. Three acoustic modes correspond to a representation Γ_4 (or T in Mulliken notation). The complex-conjugate representations Γ_2 and Γ_3 are bracketed together and labeled as a two-dimensional representation E (Mulliken notation) in Table II, because the time-reversal symmetry makes them degenerate. In all, we have the direct-sum reduction $6\Gamma_1\oplus 6\Gamma_2\oplus 6\Gamma_3\oplus 17\Gamma_4$ for the 69 optical normal modes, of which 18 are Raman active.

C. Mössbauer experiments

Figures 6(b) and 6(c) show characteristic Mössbauer spectra of the α-$SnWO_4$ powders fused in vacuum and in the argon atmosphere, respectively. For each spectrum, the Mössbauer data analysis program[15] was used to analyze the data. The small peak at around 0 mm s^{-1} was treated as a doublet and is called here the SnO_2 component, although other phases such as Sn_2O_3 and Sn_3O_4 containing Sn^{4+} ions may also result from the oxidation and decomposition of $SnWO_4$. The larger peaks in Fig. 6 were also treated as a doublet with an intensity difference in the two peaks, this ratio being called G-K (see below). The full width at the half maximum (FWHM) was set to be equal for the two doublets. The initial values for the doublet splitting ΔE_Q, the chemical isomer shift δ, the FWHM, and the intensities were given and the fittings made. The results are given in Table III.

TABLE II. Character table together with normal modes at $\mathbf{k}=\mathbf{0}$ and selection rules for β-$SnWO_4$. Bases of the irreducible representations of the point group T are also given. R and IR indicate Raman-active and IR-active modes, respectively. $\omega=\exp(-2\pi i/3)$; $t_0=(000)$; $t_1=(a/2\ a/2\ 0)$; $t_2=(a/2\ 0\ a/2)$; $t_3=(0\ a/2\ a/2)$.

Space group T^4 Irreps (and $\Delta^{(\Gamma)}$)		Basis	$\{E\|t_0\}$	$\{C_{2z}\|t_0\}$, $\{C_{2y}\|t_2\}$, $\{C_{2x}\|t_0\}$	$\{c_3^{xyz}\|t_0\}$, $\{c_3^{x\bar{y}z}\|t_2\}$ $\{c_3^{xyz}\|t_1\}$, $\{c_3^{xyz}\|t_3\}$	$\{c_3^{2xyz}\|t_0\}$, $\{c_3^{2x\bar{y}z}\|t_3\}$ $\{c_3^{2xyz}\|t_2\}$, $\{c_3^{2xyz}\|t_1\}$	Acoustic	Optic	R/IR
Group operation					Modes at $\mathbf{k}=\mathbf{0}$				
A	Γ_1		1	1	1	1		6	R
E	Γ_2		1	1	ω	ω^2		6	R
	Γ_3		1	1	ω^2	ω		6	R
T	Γ_4	x,y,z	3	-1	0	0	1	17	IR
$\Delta^{(\Gamma)}$			72	0	0	0			

The linewidth in the spectrum of the α-$SnWO_4$ powder obtained by fusion in vacuum was narrower than the one in the spectrum of the powder fused in the argon atmosphere. No significant differences were detected in the Mössbauer spectra in Fig. 7 measured in three edge directions of the cube (see Experiment). The differences were inside the margin of error, i.e., the peak asymmetry for the doublet of α-$SnWO_4$ was not due to texture effects. The fitted results for the three spectra in Fig. 7 together with fitted results for a spectrum of the thin sample (see Experiment) are also presented in Table III. The FWHM was, as expected, smaller in the spectrum of the thin sample than in the ordinary one.

Figure 6(a) shows a characteristic Mössbauer spectrum of the β-$SnWO_4$ powder. It also consists of two doublets where

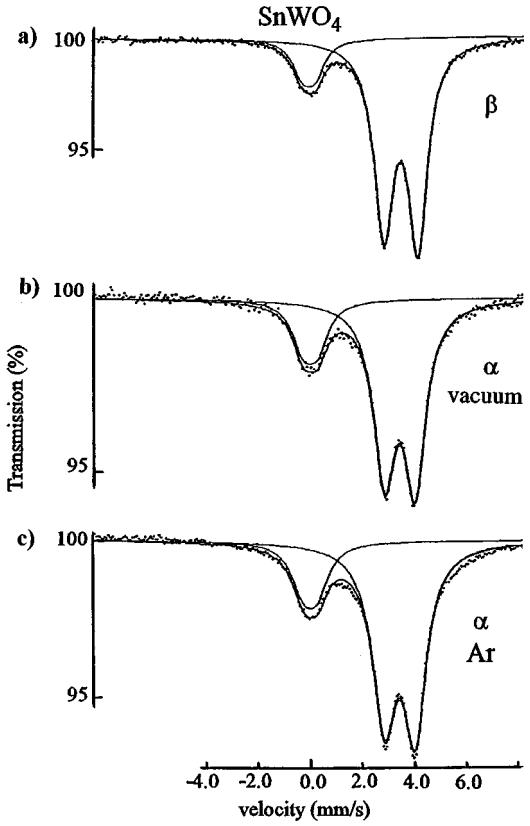

FIG. 6. ^{119}Sn Mössbauer spectra from (a) metastable β-$SnWO_4$ powder fused in vacuum and from α-$SnWO_4$ powders fused (b) in vacuum and (c) in argon.

the small peak at around 0 mm s^{-1} was treated as a doublet corresponded to the SnO_2 component and the larger peaks were also treated as a doublet with some asymmetry in their intensities (G-K ratio) belonging to the β-$SnWO_4$ phase. The FWHM was set to be equal for the two doublets and the fitted results are presented in Table III.

1. Central doublet

For all Mössbauer spectra we interpret the small doublet at around 0 mm s^{-1} to originate in some extra phase(s) containing Sn^{4+} ions. The chemical isomer shift δ is about 0.01 mm s^{-1} and its electric quadrupole splitting ΔE_Q is about 0.54 mm s^{-1} in Table III. These values are in good agreement with the published data for the crystalline SnO_2 [$\delta=0.02(2)$ mm s^{-1} and $\Delta E_Q=0.50(1)$ mm s^{-1} (Ref. 16)]. The intensity of this SnO_2 component is roughly around 18% in Table III, but the amount of this phase component is not necessarily 18%. The intensity is a product of the amount and the relevant Mössbauer recoil-free fraction f (see below). For polycrystalline SnO_2, the f factor at room temperature is reported to be 0.56.[16] The values of the f factor for the $SnWO_4$ phases are unknown in the literature, but the calculations done here using reported x-ray temperature factors (see below) gave values of around 0.16–0.20 for the f factors. Using these values and 0.56 for the SnO_2 component gives around 7% for the amount of the extra phase(s).

In the case of very small grains of the extra phase(s) at the surface of the $SnWO_4$ matrix, it is not possible to see their reflections in the XRD patterns. However, they may have a strong influence on the chemical surface properties. In conversion electron Mössbauer spectra (CEMS) from α-$SnWO_4$ thin films, made by sputtering, the central doublet was much higher than the doublet from the α-$SnWO_4$ phase after annealing the films at 400 °C.[3] However, in the XRD patterns of the films there were high reflections only from the α phase and very small reflections from SnO_2 and some other phases. The reason may relate to the fact that CEMS gives information which is more surface sensitive and sputtered surfaces are more sensitive to decompose during annealing. Large differences were found in the gas-response properties between α-$SnWO_4$ thin films, made by sputtering, and thick-films, made by screen printing from fused powders, with similar XRD patterns but very different Mössbauer spectra.[3]

TABLE III. Results from the fitting of Mössbauer spectra for Sn^{4+} and Sn^{2+} cations in various α- and β-$SnWO_4$ powder samples (see Experiment). FWHM is for the linewidth, I is for the fractional intensity between Sn^{4+} and Sn^{2+} doublets, δ is for the chemical isomer shift, ΔE_Q is for the electric quadrupole splitting, and G-K is the intensity ratio of the Sn^{2+} doublet.

	Parameters for Sn^{4+}				Parameters for Sn^{2+}			
Sample	FWHM (mm s^{-1}) ± 0.01	I (%) ± 1.0	δ (mm s^{-1}) ± 0.02	ΔE_Q (mm s^{-1}) ± 0.03	I (%) ± 1.0	δ (mm s^{-1}) ± 0.01	ΔE_Q (mm s^{-1}) ± 0.01	G-K ± 0.02
β-$SnWO_4$	0.47	14.0	−0.01	0.49	86.0	3.50	1.30	1.08
α-$SnWO_4$ (argon)	0.66	19.5	0.03	0.52	80.5	3.42	1.18	1.08
α-$SnWO_4$ (vacuum)	0.58	19.7	0.02	0.55	80.3	3.42	1.18	1.06
α-$SnWO_4$ (cube x)	0.60	18.8	0.03	0.59	81.2	3.43	1.18	1.08
α-$SnWO_4$ (cube y)	0.63	18.6	0.01	0.56	81.4	3.43	1.18	1.09
α-$SnWO_4$ (cube z)	0.63	18.6	0.02	0.50	81.4	3.43	1.18	1.06
α-$SnWO_4$ (thin sample)	0.46	18.8	0.01	0.54	81.2	3.43	1.16	1.08

2. Goldanskii-Karyagin effect in α-$SnWO_4$

The peak-intensity asymmetry is most probably due to the Goldanskii-Karyagin effect.[17] The Mössbauer spectra for the α phase in Figs. 6(b) and 6(c) are very similar irrespectively if the samples were fused in vacuum or in argon, consequently we can deal with them together. From the anisotropic temperature-factor coefficients β_{ij} [Eq. (3)] in Ref. 5 for the Sn atom in α-$SnWO_4$ it is possible to calculate the mean-square displacement matrix B [Eq. (1)] and diagonalize it to get B' with $B'_{11}=\langle u^2_{x'}\rangle$, $B'_{22}=\langle u^2_{y'}\rangle$, and $B'_{33}=\langle u^2_{z'}\rangle$ to represent the principal axes components of the vibrational ellipsoid in the new coordinate system (x',y',z'):

$$B'=\begin{pmatrix} 1735.0 & 0 & 0 \\ 0 & 1006.96 & 0 \\ 0 & 0 & 712.28 \end{pmatrix} 10^{-5}\text{Å}^2, \qquad (6)$$

The diagonalization in Eq. (6) means a rotation around the unit-cell **c** axis of the α-$SnWO_4$ structure and z' and **c** axes are parallel. Figure 8 shows a projection of the distorted SnO_6 octahedron in the unit-cell coordinate system of α-$SnWO_4$. The lone-pair orbital of Sn is in the direction of the z axis. Since the lone pair has the strongest effect in the electric-field-gradient (EFG) tensor it can be considered that the principal axis of the EFG tensor coincides with the **c** axis of the unit cell.

Since a principal axis of the mean-square displacement matrix B' is now parallel to the principal axis of the EFG tensor, a general formula for the ratio between the intensities in the two peaks of the Mössbauer doublet for a nonsymmetric electric-field gradient is[18]

$$\frac{I_l}{I_2}=\frac{\int\int P_l(\theta,\varphi)h(\theta)f(\theta,\varphi)\sin\theta\, d\theta d\varphi}{\int\int P_2(\theta,\varphi)h(\theta)f(\theta,\varphi)\sin\theta\, d\theta d\varphi}, \qquad (7)$$

where $h(\theta)=1$ in the case of no texture.[19] The quantities $P_1(\theta,\varphi)$ and $P_2(\theta,\varphi)$ are the relative angular-dependent absorption probabilities for the transitions $(1/2,\pm 1/2)\rightarrow(3/2,\pm 3/2)$ and $(1/2,\pm 1/2)\rightarrow(3/2,\pm 1/2)$, respectively. In the

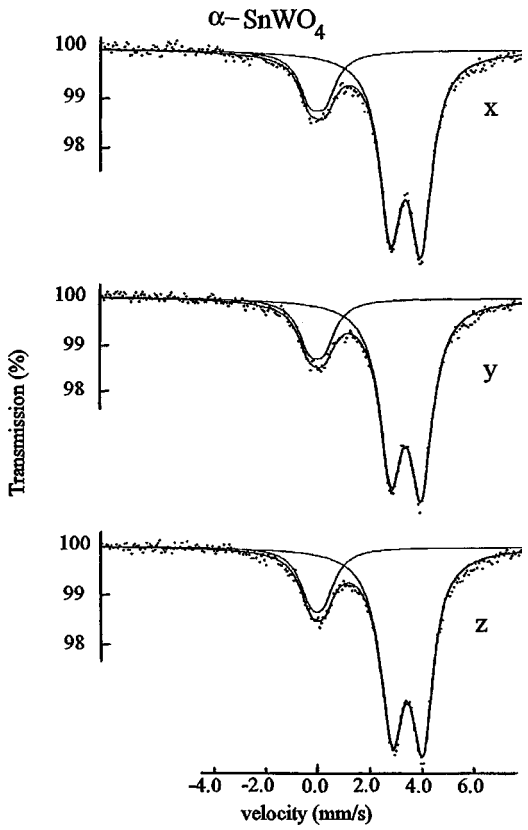

FIG. 7. ^{119}Sn Mössbauer spectra from a cubic α-$SnWO_4$ powder (fused in vacuum) sample measured in the three cube directions x, y, and z.

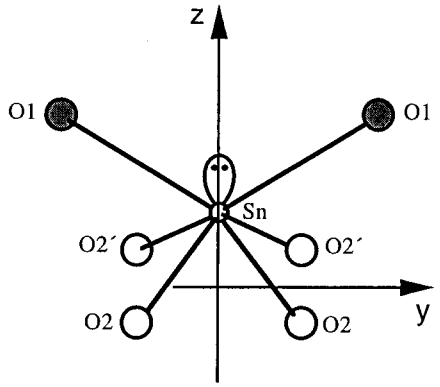

FIG. 8. Projection of the distorted SnO_6 octahedron around the lone-pair tin cation in α-$SnWO_4$. The lone pair is in the z direction (parallel to the z' and **c** axes) and is marked by two dots.

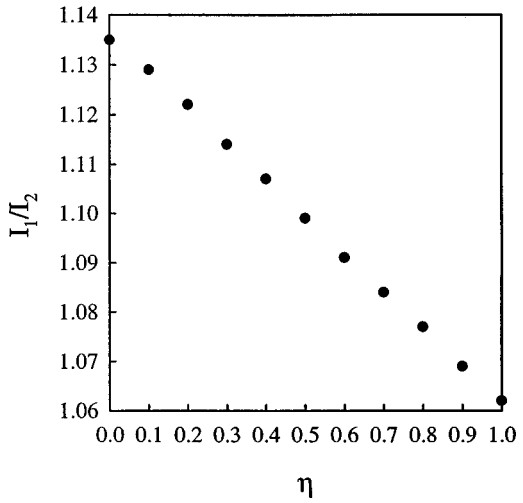

FIG. 9. The intensity ratio I_1/I_2 for the two peaks in the Mössbauer doublet of α-$SnWO_4$, calculated as a function of the asymmetry parameter η from Eq. (7).

case of a randomly oriented crystal the transition probabilities are

$$P_1(\theta,\varphi)=4\sqrt{1+\frac{\eta^2}{3}}+(3\cos^2\theta-1+\eta\sin^2\theta\cos 2\varphi),$$

$$P_2(\theta,\varphi)=4\sqrt{1+\frac{\eta^2}{3}}-(3\cos^2\theta-1+\eta\sin^2\theta\cos 2\varphi), \tag{8}$$

where η is the asymmetry parameter. For a positive value of the electric quadrupole splitting $\Delta E_Q=1/2eQV_{zz}$, P_1 corresponds to a higher energy and thus to a larger velocity in the spectrum. For the γ-photon direction (θ, φ) the recoil-free fraction is given as

$$f(\theta,\varphi)=\exp\{-k^2[(\langle u_{x'}^2\rangle\cos^2\varphi+\langle u_{y'}^2\rangle\sin^2\varphi)\sin^2\theta+\langle u_{z'}^2\rangle\cos^2\theta]\}, \tag{9}$$

The wave vector is here $k=E_{\rm ph}(\hbar c)=12.0908\ \text{Å}^{-1}$ using the value $E_{\rm ph}(^{119}\text{Sn})=23.875$ keV of the γ-ray transition for ^{119}Sn. The average recoil-free fraction f can be calculated by numerical integration of Eq. (9), and the use of the diagonal elements of the matrix B' in Eq. (6) gave $f=0.20$.

The integrals in Eq. (7) were calculated for different values of the asymmetry parameter η between 0 and 1 and the ratios I_1/I_2 (Fig. 9) were obtained as a function of η. The experimental asymmetry of about 1.08 for α-$SnWO_4$ in Table III corresponds well with the calculated values that ranges from 1.06 to 1.14 in Fig. 9. The experimental average value of 1.08 corresponds to a value of 0.75 for η in Fig. 9. Furthermore, we can conclude that ΔE_Q is positive. Since the nuclear quadrupole moment Q is negative for ^{119}Sn the electric-field gradient V_{zz} is also negative.

3. Goldanskii-Karyagin effect in β-SnWO₄

The Mössbauer doublet of β-$SnWO_4$ in Fig. 6(a) is also asymmetric due to the Goldanskii-Karyagin effect. The tin environment is also now a distorted octahedron as is shown in Fig. 2. From the anisotropic temperature-factor coefficients β_{ij} in Ref. 1 for the Sn atom it is possible to calculate the mean-square displacement matrix B and diagonalize it into the form

$$B'=\begin{pmatrix}1408.82 & 0 & 0\\ 0 & 1408.82 & 0\\ 0 & 0 & 955.4\end{pmatrix}10^{-5}\text{Å}^2. \tag{10}$$

The principal axis z' of the vibrational ellipsoid is in the [111] direction in the unit-cell cube. The average recoil-free fraction f can be calculated by numerical integration of Eq. (9) and the diagonal elements of the matrix B' in Eq. (10) gave $f=0.16$.

Figure 10 shows a projection of the distorted oxygen octahedron surrounding the lone-pair tin cation in the β-$SnWO_4$ structure. The lone-pair orbital of the Sn cation is along the z' ([111]) direction, and as in the α phase the principal axis of the EFG tensor coincides with the principal z' axis of the vibration ellipsoid. Through the Sn position on

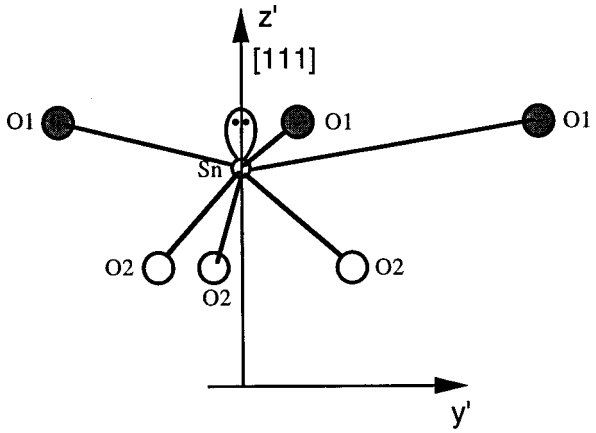

FIG. 10. Projection of the distorted SnO_6 octahedron around the lone-pair tin cation in β-$SnWO_4$. The lone pair is in the z' direction which is parallel to the [111] direction in the unit cell and is marked by two dots.

the cube diagonal in the β-$SnWO_4$ structure, the cylindrical symmetry gives the value zero for the asymmetry parameter η.

The intensities of the two peaks of the asymmetric doublet can now be calculated by the numerical integration of the integrals in Eq. (7) and the results are $I_1=8.547$ and $I_2=7.785$, so the ratio $I_1/I_2=1.098$. The experimental asymmetry of 1.08 reported for β-$SnWO_4$ in Table III corresponds well with the calculated value. Also here are $\Delta E_Q>0$ and $V_{zz}<0$ as for α-$SnWO_4$.

4. Electric quadrupole splittings and chemical isomer shifts

The obtained experimental values for the chemical isomer shift δ and electric quadrupole splitting ΔE_Q in the α- and β-$SnWO_4$ structures compares well with the values reported by Ballard and Birchall.[20] For the α phase there are two oxygen atoms at 2.82 Å [O(1)], two oxygen atoms at 2.18 Å [O(2)] and two oxygen atoms at 2.39 Å [O(2′)] around the lone-pair tin cation in Fig. 8. The $5s$ electrons in Sn are thus not bare, but take part in the bonding. The electric quadrupole coupling in covalent tin systems is almost entirely made up by the imbalance in the population of the p orbitals and the electron density on the surrounding atoms and ions can be ignored.[21]

The electric quadrupole moment Q is negative and the electric quadrupole splitting for Sn has been approximated with the expression[22]

$$\Delta E_Q=+4.0[n_z-0.5(n_x+n_y)]\text{mm s}^{-1}, \tag{11}$$

where n_x, n_y, and n_z are the populations of different p orbitals.

The chemical isomer shift depends on the electron density at the nucleus, and for Sn general formulas have been obtained.[21,22] Flinn[23] has suggested the following formula for the chemical isomer shift with the absorber and source at 77 K:

$$\delta(\text{vs BaSnO}_3)\approx[3.01n_s-0.20n_s^2-0.17n_sn_p-0.38]\text{m s}^{-1}, \tag{12}$$

where n_s and n_p are the $5s$- and $5p$-electron populations. In the case here, the δ versus $CaSnO_3$ and with the absorber and source at room temperature is reported. Assuming the same Debye temperature for the two tin oxides involved this formula can also be used up to room temperature. In this case stannous ions are assumed, i.e., $n_s+n_p=2$. Furthermore, $n_p=(n_x+n_y)+n_z$. There are now four equations with four variables n_s, n_p, n_x+n_y, and n_z. The populations can be calculated and the results are $n_s=1.45$, $n_p=0.55$, $n_x+n_y=0.17$, and $n_z=0.38$. The results are in agreement with the lone-pair drawing in Fig. 8.

For the β phase there are three oxygen atoms at 2.21 Å [O(2)] and also three at 2.81 Å [O(1)] around the lone-pair Sn cation in Fig. 10. Similarly, as in the α phase above, the populations for the $5s$ and $5p$ electrons in β-$SnWO_4$ can be calculated. The β phase has cylindrical symmetry around the Sn cations and $n_x=n_y$. The results for the population of the $5s$ and $5p$ electrons are $n_s=1.48$, $n_p=0.52$, $n_x=n_y=0.065$, and $n_z=0.39$. Again, the results are in agreement with the lone-pair drawing in Fig. 10. The withdrawal of $5s$ electrons from Sn is larger for Sn in the α phase than in the β phase, as expected from the surrounding oxygen octahedra in Figs. 8 and 10.

V. CONCLUSIONS

^{119}Sn Mössbauer and Raman spectroscopies together with x-ray-diffraction measurements were used to study the phase structure of $SnWO_4$ powders fused from SnO and WO_3 powders in vacuum and in argon into the α- and β-$SnWO_4$ phases. X-ray-diffraction patterns were incapable to reveal small extra phase(s) from the oxidation of Sn^{2+} ions into the Sn^{4+} form in the α- and β-phase powders. Raman spectroscopy as a local probe was also insensitive to expose the extra phase component(s) in the powders. The reason may be in the low intensities of Raman peaks in spectra from various tin oxides such as SnO and SnO_2. Mössbauer spectroscopy, on the other hand, is sensitive to changes in the valence state and bonding and revealed clearly the extra phase(s) containing Sn^{4+} ions in the powders. An asymmetry was found between the two peaks in the Mössbauer doublet at both $SnWO_4$ phases and it was possible to relate the asymmetry to the Goldanskii-Karyagin effect in both α and β phases. The values 0.20 and 0.16 were calculated for the average recoil-free fraction f from published thermal parameters for α and β phases respectively, and a value of around 0.75 was obtained for the asymmetry parameter η in α-$SnWO_4$. The $5s$- and different $5p$-electron populations in the stannous ions in the α- and β-phase structures were calculated from the obtained values for the electric quadrupole splitting and chemical isomer shift, and the results exposed the lone-pair character of the tin cations in both phases. Raman spectra are also given for both α- and β-phase powders together with peak frequencies from a curve fit. Normal-mode symmetries together with selection rules are also given for α- and β-$SnWO_4$ at $\mathbf{k}=\mathbf{0}$.

ACKNOWLEDGMENTS

J.S. expresses his gratitude to International Science Programs at the Uppsala University, Sweden for the financial support. Additional support was received from the Academy of Finland.

*Permanent address: Universidad Nacional de Ingenieria, Facultad de Ciencias, P.O. Box 31-139, Lima, Peru.

[1] W. Jeitschko and A. W. Sleight, Acta Crystallogr., Sect. B: Struct. Crystallogr. Cryst. Chem. **28**, 3174 (1972).

[2] J. L. Solis and V. Lantto, Phys. Scr. **T69**, 281 (1997).

[3] J. L. Solis, V. Lantto, L. Häggström, and M. Wikner, Hyperfine Interact. **2**, 256 (1997).

[4] J. L. Solis and V. Lantto, Sens. Actuators B **24–25**, 591 (1995).

[5] W. Jeitschko and A. W. Sleight, Acta Crystallogr., Sect. B: Struct. Crystallogr. Cryst. Chem. **30**, 2088 (1974).

[6] V. Lantto, in *Gas Sensors*, edited by G. Sberveglieri (Kluwer, Dordrecht, 1992).

[7] C. G. Granqvist, *Handbook of Inorganic Electrocrhomic Materials* (Elsevier, Amsterdam, 1995).

[8] J. Frantti and V. Lantto, Phys. Rev. B **56**, 221 (1997).

[9] J. L. Solis, J. Frantti, and V. Lantto, in *Surfaces, Vacuum, and*

Their Applications, edited by I. Hernández-Calderón and R. Asomoza, AIP Conf. Proc. No. **378**, (AIP, New York, 1996), pp. 169–176.

[10] B. T. M. Willis and A. W. Pryor, *Thermal Vibrations in Crystallography* (Cambridge University Press, Cambridge, 1975).

[11] T. Ericsson and R. Wäppling, J. Phys. (Paris), Colloq. **37**, C6-719 (1976).

[12] J. L. Birman, in *Encyclopedia of Physics*, edited by S. Flugge and L. Genzel (Springer, Berlin, 1974).

[13] J. F. Cornwell, *Group Theory and Electronic Energy Bands in Solids* (Elsevier, New York, 1974).

[14] M. Tinkham, *Group Theory and Quantum Mechanics* (McGraw Hill, New York, 1964).

[15] P. Jernberg and T. Sundqvist, Uppsala University, Report No. UUIP-1090, 1983 (unpublished).

[16] B. Stjerna, C. G. Granqvist, A. Seidel, and L. Häggström, J. Appl. Phys. **68**, 6241 (1990).

[17] S. V. Karyagin, Dokl. Akad. Nauk SSSR **148**, 1102 (1963); V. I. Goldanskii, E. F. Makarov, and V. V. Khrapov, Phys. Lett. **3**, 344 (1963).

[18] P. Gütlich, R. Link, and A. Trautwein, *Mössbauer Spectroscopy and Transition Metal Chemistry* (Springer, Berlin, 1978), p. 34.

[19] P. Zory, Phys. Rev. **140**, A1401 (1965).

[20] J. G. Ballard and T. Birchall, Can. J. Chem. **53**, 3371 (1975).

[21] R. V. Parish, Mössb. Eff. Ref. Data J. **5**, 196 (1982).

[22] R. V. Parish, in *Mössbauer Spectroscopy Applied to Inorganic Chemistry*, edited by G. J. Long (Plenum, New York, 1984), Vol. 1, p. 527.

[23] P. A. Flinn, in *Mössbauer Isomer Shift*, edited by G. K. Shenoy and F. W. Wagner (North-Holland, Amsterdam, 1978), p. 593.